AIAA SciTech Forum
7-11 January 2019, San Diego, California
AIAA Scitech 2019 Forum

10.2514/6.2019-1746

Analysis of the Column Bending Test for Bending of High Strain Composites

Ajay Harihara Sharma *
University of Colorado, Boulder, Colorado, 80309, USA

TJ Rose †
Roccor, LLC, Longmont, CO 80503
University of Colorado, Boulder, Colorado, 80309, USA

Andrew Seamone ‡
University of Colorado, Boulder, Colorado, 80309, USA

Thomas W. Murphey §
Opterus Research and Development Inc, Fort Collins, CO 80526, USA

Francisco López Jiménez¶
University of Colorado, Boulder, Colorado, 80309, USA

High Strain Composites (HSCs) already play a crucial role in the design of several deployable space structures, but their application in new designs is hindered by the lack of understanding of the mechanics controlling their failure properties. Several recent studies have focused on the development of new set of testing and modeling standards for HSCs, particularly under bending. This paper aims to contribute to this effort by analyzing the Column Bending Test (CBT), currently the preferred method to study the moment-curvature behavior and failure curvature of HSCs, since it can apply a relatively constant bending moment until very high curvatures. In particular, we quantify the errors involved in the simplified geometric analysis often used to model the CBT, by considering two different effects: variations in the bending moment through the sample and non-linearities in the material response of the fibers. The first effect, modeled using Euler's elastica, results in a set of design guidelines for the test geometry (*i.e*, length of the grips and the specimens) in order to achieve moderate errors in the curvature prediction. The non-linearities in the fiber behavior (tension stiffening and compression softening) does not have a strong effect on the curvature, but produces significant variations in the maximum strain observed in the fibers, due to the shift in the neutral axis. This indicates that accounting for the nonlinear behavior of fibers is necessary in order to accurately predict the failure properties of HSCs under bending.

I. Introduction

Several designs of deployable space structures are based on the elastic deformation of structural elements during stowage, and the subsequent deployment by releasing the stored strain energy. Examples include continuous longeron masts (CLM) [1], antenna booms [2], spring-back reflector [3], large deployable antennas [4], tape-spring truss [5], deployable solar arrays [6]. In order to further increase their packaging efficiency, these architectures often rely on High Strain Composites (HSC) [7], a class of fiber composite structures designed to operate at strains higher than 1%, usually through folding at large curvatures. Despite their promising mechanical properties, the application of HSC is

*Graduate Student, Ann and H.J. Smead Department of Aerospace Engineering Sciences, University of Colorado, Boulder, AIAA Student Member

†Sr. Mechanical Engineer, Roccor, LLC, Longmont, CO 80503 ; Graduate Student, Ann and H.J. Smead Department of Aerospace Engineering Sciences, University of Colorado, Boulder, AIAA Member.

‡Undergraduate Student, Department of Civil, Environmental and Architectural Engineering , University of Colorado, Boulder

§President. Opterus Research and Development Inc, 4221 Rolling Gate Rd, Fort Collins, CO, AIAA Associate Fellow

¶Assistant Professor, Ann and H.J. Smead Department of Aerospace Engineering Sciences, University of Colorado, Boulder, AIAA Member.

hindered by the lack of analytical and numerical tools able to reliably and accurately predict their failure curvature, as well as their behavior after the long stowage periods expected in a space mission. In order to shed light on the unique micromechanics taking place in HSC, several recent studies have focused on the testing of their large curvature bending behavior [8–21]. A key goal of this experimental campaign is the development of a reliable and well characterized testing standard.

The experimental determination of the high curvature bending behavior of HSC, including their failure curvature, requires a testing procedure able to subject thin composite laminates to very high curvatures, sometimes in the range $\kappa > 0.4$ mm^{-1}. Traditional bending testing techniques, such as three- and four-point bending, are only valid in the linear regime, and therefore insufficient for the present goals. Several alternative techniques have been explored. The Large Deformation Four Point Bending Test is able to produce the required high curvatures, but the abrupt transition of the stress state at the grips leads to premature failure of the coupons [12]. The platen test has also been used to test the failure curvature of thin composite laminates [11], but the moment distribution throughout the specimen is highly non-uniform, leading to large errors in the processing of results unless the large deformation behavior is modeled correctly.

The Column Bending Test (CBT) [13–19] is able to overcome these two shortcomings, loading the coupons with a nearly constant bending moment that results in failure close to the center of the coupon. The setup can be seen in Fig. 1. The test uses pins to turn rotation into bending moment, and arms to increase distance so that moment is almost constant. If the coupon is sufficiently shorter compared to the length of the arms, the variation of the bending moment within the specimen is small, which results in close to uniform curvature, and makes it possible to analyze the test using simple geometric arguments. However, the minimum length of the coupon depends on both the size of the arm and the maximum curvature expected during the test, and so sometimes the variations of curvature within coupons are significant, particularly between samples of different thickness.

The objective of the present study is to evaluate the validity of the usual assumptions used to process the results of the CBT test. In particular, we will compare the maximum curvature calculated using a closed form solution derived geometrically by assuming constant curvature through the specimen, with the prediction obtained analyzing the test using Euler's elastica theory, which models the behavior of rods subjected to large deflections. Our results provide the error between both predictions as a function of the main geometry parameters of the test (size of the grips and free length of the tested coupon), and they can be used to determine when a simple geometrical analysis is able to produce an accurate prediction of the maximum curvature in the specimens. Moreover, we also investigate the effect of nonlinearity in the fiber stiffness on the mechanics of the laminate, such as quantifying the shift of neutral axis and its effect on stresses and strains. We also present the experimental validation of our analysis using image processing of test images.

The structure of the paper is as follows. Section II provides a background of the Column Bending Test. Section III explains the model used to capture possible nonlinearities in the fiber behavior. In Section IV, we then explain the elastica theory that is used to predict the variations in curvature across the specimen. Section V discusses the comparison of curvature predictions obtained through the closed form solution, and the elastica theory for various cases of softening observed in HSCs, while Section VI discusses the effects of softening on the local stresses and strains in the fiber. Finally, preliminary experimental validation is presented in Section VII.

II. Background of Column Bending Test

The main objective of Column Bending Test is to obtain the moment versus curvature behaviour in the geometrically nonlinear regime for various HSC materials and laminate layups. The slope of moment versus curvature curve provides the value of bending stiffness (D_{11}) for a particular choice of layup as a function of the applied curvature, revealing possible material non-linearities. The test also provides the failure curvature of the material, which is one of the main parameters necessary for the design of deployable space structures using HSC. The goal of this section is to review the experimental setup, and the closed form that can be developed assuming constant curvature in the sample.

A. Description of the experimental setup

The CBT is designed to characterize the bending behavior of thin coupons at large curvatures in an universal testing machine. In order to effectively transmit the loading applied by the testing machine into bending moment in the samples, the CBT fixture holds the specimens using rigid arms. One end of the rigid arm is attached to the specimen, and the other end is pinned to a U-shaped clevis attached to the testing machine. In order to reduce friction, bearings are

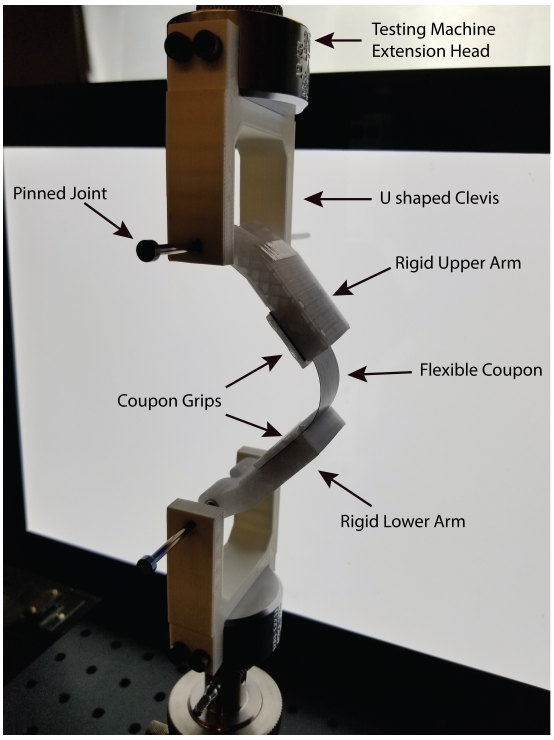

Fig. 1 Image of the experimental setup used in the Column Bending Test.

attached at the location where the U-shaped clevis and the rigid arms meet, so that a rod can transmit the force between the two pieces, and freely rotate on the bearings. At the other end of the rigid arm, a rigid grip plate allows the specimen to be sandwiched between the plate and the arm. A shimstock is also sandwiched in this region along with the specimen so as to prevent warping of the specimen or the rigid arm plate, as the test proceeds. Since the loads observed in the test are usually small, it is important to reduce the effect of the gravity. Two strategies are commonly used for the same. First, the fixture is usually built with polymers through rapid prototyping. Second, the fixture can be designed using arms that are symmetric around their connection to the rod, so that they are balanced in the absence of loading, see Fig. 2.

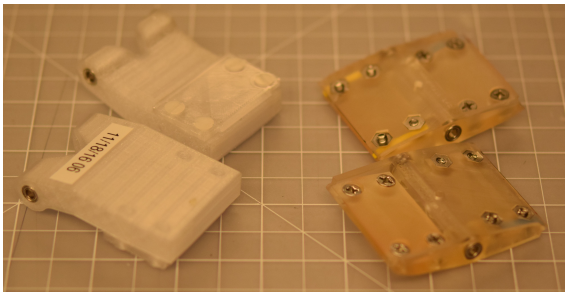

Fig. 2 Example of unbalanced (left) and balanced (right) grips used in CBT, provided by Opterus Research and Development Inc.

If the specimen is initially straight and aligned with the loading axis, the loading will first compress the coupon until buckling takes place resulting in bending of the specimen. In order to facilitate the test, it is important to ensure that the coupon bends in a previously determined direction. Two alternatives can be used. First, the test can be started with the coupon already buckled, introducing a small initial curvature. Alternatively, the coupons are offset from the loading axis (*i.e.*, the pinned joints where the arms meet the U-shaped clevis) by a small distance, so that a small bending moment is introduced at the beginning of the test. Regardless of the approach followed, as the test progresses the distance between sample and loading axis increases rapidly, and the axial and shear loading in the coupon can be neglected compared to

the bending moment.

B. Geometric analysis

During the CBT test the bending moment along the coupon varies linearly with the distance to the loading axis, with the minimum at the grip and the maximum and the center of the specimen. If the relative difference between both distances is small and the material properties are linear, it is possible to assume that the bending moment, and therefore the curvature, is close to constant along the arc length. It is also assumed that the length of the specimen remains constant during the test, since the compressive loading is neglible compared to the bending moment. This greatly simplifies the analysis of the test, and it is possible to provide a closed form estimation of the maximum curvature and bending moment. The main objective of this paper is to explore the regime where this assumption yields accurate results. The geometric closed form solution has already been previously discussed [18, 19], but it will be also presented here for completion.

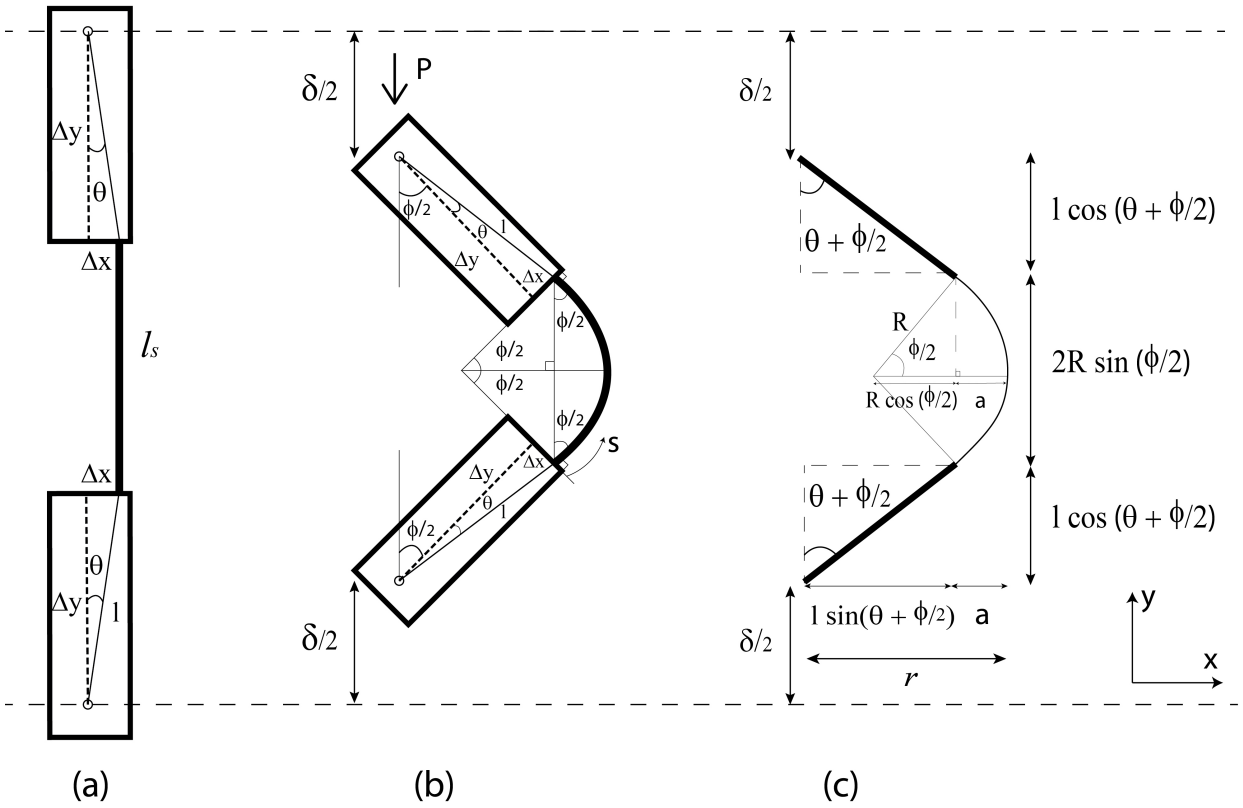

Fig. 3 Geometry of the Column Bending Test: (a) Initial test geometry, (b) Angles and (c) Distances in the test setup when a displacement δ is applied.

In Figure 3, l_s represents the free length of the samples between the rigid arms or gauge length (assumed to be constant during the test), l represents the effective length of the rigid fixture arm (*i.e.*, the distance between sample and pin), θ represents the initial angle of the fixture arm, ϕ represents the change in fixture arm angle due to deflection during the test, δ represents the linear vertical displacement of the fixture, P represents the load applied by the testing machine to the fixture, r represents the effective moment arm length, a represents the horizontal component of the distance between center and end of the coupon, and R represents the radius of curvature of the bent coupon.

From Figure 3a, we can see that the position of the pinned joint and the position from where the specimen leaves the rigid arm are offset. This distance is given by Δx. As mentioned above, this offset parameter helps ensure that the

specimen always bends in the desired direction as the test proceeds. An assumption made here is that the specimen leaves the rigid arm at a perfect 90° angle. As a result of this assumption, the sum of the angles by which the two rigid arms rotate (ϕ) is the same angle which is subtended by the arc at the center of the assumed circle. This greatly simplifies the calculations, since curvature can now be obtained using the radius of curvature (R), freelength (l_s) and the central angle (ϕ).

In order to evaluate the central angle (ϕ), we can write an expression that involves conservation of the vertical distance before and during the test (see Fig.3). The initial vertical distance involves contributions from the free length (l_s) and vertical component of the rigid arms. It is given by:

$$d_{initial} = 2l\cos\theta + l_s \tag{1}$$

When each of the arms undergoes an angular rotation of ($\phi/2$) as a results of the vertical displacement δ, the total vertical distance is then given by:

$$d_{final} = \delta + 2R\sin(\phi/2) + 2l\cos(\theta + \phi/2) \tag{2}$$

Upon applying $d_{initial} = d_{final}$, we get:

$$\frac{\delta}{l_s} = 1 - \frac{2}{\phi}\sin\frac{\phi}{2} + 2\frac{l}{l_s}\left(\cos\theta - \cos\left(\theta + \frac{\phi}{2}\right)\right) \tag{3}$$

The above equation for ϕ is transcendental and requires a numerical solution. As mentioned above, the curvature can now be obtained using the definition of curvature, $\kappa = \frac{1}{R}$, and the formula for arclength of a circle, $l_s = R\phi$, yielding:

$$\kappa = \frac{\phi}{l_s} \tag{4}$$

In order to compute the maximum moment M_{max}, it is essential to first obtain the effective moment arm length r. As seen from Figure 3c, the distance r can be given by:

$$r = a + l\sin(\theta + \frac{\phi}{2}) \tag{5}$$

From Figure 3c, we can also see that:

$$a = R - R\cos\left(\frac{\phi}{2}\right) \tag{6}$$

Substituting the expression of a in the expression for r and dividing it by s, we obtain:

$$\frac{r}{s} = \frac{1}{\phi}\left(1 - \cos\frac{\phi}{2}\right) + \frac{l}{s}\sin\left(\theta + \frac{\phi}{2}\right) \tag{7}$$

Assuming that the neutral axis always remains at the center of the specimen during bending, the strain can be calculated using the curvature κ and thickness t and is given by:

$$\varepsilon = \frac{\kappa t}{2} \tag{8}$$

The maximum moment occurs at the center of the specimen and is given by:

$$M_{max} = Pr \tag{9}$$

The minimum moment occurs at the coupon edges near the grips. It is given by:

$$M_{min} = Plsin(\theta + \frac{\phi}{2}) \tag{10}$$

Next, we consider two ways in which the reality deviates from the simplified geometric analysis. First, the effect of material nonlinearities is discussed. After that, the effect of non constant curvature is discussed by utilizing the theory of elastica.

III. Mechanics of High Strain Composites

Ever since the recognition of the non-linear behavior of carbon fibers, several constitutive models have been proposed to determine their behavior under large deformations [22–24]. After performing an extensive investigation of these models, Murphey et.al.[20] developed a non-linear fiber based constitutive model to describe the behavior of thin flexures subjected to large strains. According to this model, only the fiber component is assumed to be non-linear, whereas the matrix behavior is assumed to be linearly elastic for all strains. The fiber modulus according to this model is given by:

$$E_{fT}(\varepsilon) = E_o(1 + \gamma_T \varepsilon) \quad for \quad \varepsilon \geq 0 \tag{11}$$

$$E_{fC}(\varepsilon) = E_o(1 + \gamma_C \varepsilon) \quad for \quad \varepsilon < 0 \tag{12}$$

where γ_T and γ_C represent the tensile and compressive fiber non-linear parameters respectively, and E_o represents the initial fiber modulus at zero strain. In order to obtain the overall modulus of the composite, the fiber modulus can be substituted into the rule of mixtures, given by:

$$E_c = E_f V_f + E_m(1 - V_f) \tag{13}$$

Thus, we obtain different composite modulii for tension and compression, given by:

$$E_{cT} = E_o(1 + \gamma_T \varepsilon)V_f + E_m(1 - V_f) \quad for \quad \varepsilon \geq 0 \tag{14}$$

$$E_{cC} = E_o(1 + \gamma_C \varepsilon)V_f + E_m(1 - V_f) \quad for \quad \varepsilon < 0 \tag{15}$$

Here, E_m represents the matrix modulus and V_f represents the fiber volume fraction of the composite. It can be seen from Equations 14 and 15 that the composite behaves differently under tension ($\varepsilon > 0$) and compression ($\varepsilon < 0$). In particular, for $\gamma_T > 0$ and $\gamma_C > 0$, there is stiffening under tension and softening under compression.

In order to fully characterize the non-linear behavior of an HSC at high strains, these five parameters E_m, E_o, V_f, γ_T, γ_C need to be determined. Here, we will make certain assumptions in order to simplify the constitutive model. First, the axial modulus (E_1) is assumed to be significantly larger than the transverse modulus (E_2) for the composite. This allows us to neglect the contribution of E_2 in our Moment-Curvature relationship as well as the expression for (D_{11}). Second, the nonlinear fiber parameters in tension and compression are assumed to be equal ($\gamma_T = \gamma_C = \gamma$). Third, the bending behavior for the thin flexure is solely driven by fibers ($E_c = E_f$). This results in a single equation for the fiber modulus given by:

$$E_f(\varepsilon) = E_o(1 + \gamma\varepsilon) \tag{16}$$

Using the above assumptions, we can deduce a few observations. Since the fiber modulus represents slope of the stress-strain curve, integration of the expression for E_f with respect to ε gives the constitutive relation. This yields a parabolic expression for stress (see Figure 4) given by:

$$\sigma_c = E_o\varepsilon + \frac{E_o\gamma\epsilon^2}{2} \tag{17}$$

We can also infer that for tension ($\varepsilon > 0$), the slope i.e. fiber modulus increases and for compression ($\varepsilon < 0$), the fiber modulus decreases. This phenomenon, also known as tensile stiffening and compression softening respectively, results in shifting of neutral axis towards the tension side of the specimen under bending, which ultimately results in higher strains on the compression side with respect to the tension side. Furthermore, according to this constitutive model, there also exists a critical compressive strain ($\varepsilon_{C,cr} = \frac{-1}{\gamma}$) where the instantaneous modulus becomes zero (marked with a star symbol in Figures 4 and 5). Beyond this point, the modulus becomes negative, until eventually tension is observed on the compressive side (see Figure 4). Since this is unphysical, we stop the calculations when $\varepsilon_{C,cr}$ is reached in Sections V and VI.

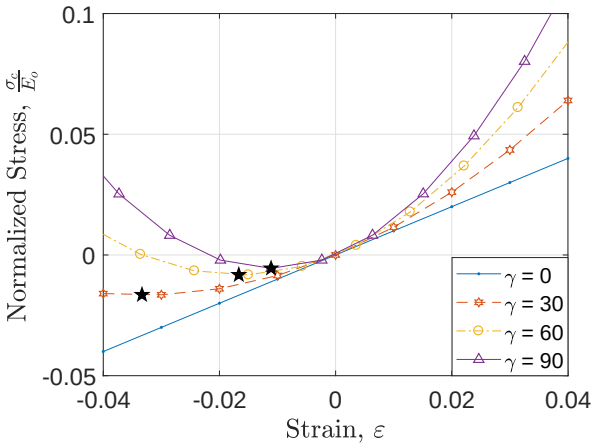

Fig. 4 Normalized stress vs. strain for four different values of the parameter γ describing fiber nonlinearity. The star represents the point at which the instantaneous modulus becomes zero. The case with γ = 0 represents the linear case where no softening is observed.

Utilizing the above assumptions, we can develop a simplified expression for the Moment-Curvature relationship, the bending stiffness(D_{11}), and the expression that quantifies the shift in neutral axis. In order to do so, we first utilize the equilibrium of internal forces through the thickness, to determine the position of the neutral axis. This is given by :

$$N_c = \int_{-t/2}^{t/2} \sigma_c \, \mathrm{d}y = 0 \tag{18}$$

Here, the stress (σ_c) is a function of the strain (ε) given by the constitutive relationship (Equation 17) . Hence, we need to determine the strain as a function of the thickness co-ordinate in order to establish the equilibrium of the forces through the thickness. Using Euler-Bernoulli theory, we obtain the relation :

$$\varepsilon = \kappa(y - y_{na}) \tag{19}$$

where y_{na} is the position of the neutral axis. Solving equations 17 , 18, and 19 gives the expression for neutral axis. This is given by :

$$y_{na} = \frac{6 - \sqrt{36 - 3t^2\gamma^2\kappa^2}}{6\gamma\kappa} \tag{20}$$

The bending moment per unit width can be evaluated using the following relation :

$$M = \int_{-t/2}^{t/2} \sigma_c (y - y_{na}) \, \mathrm{d}y = 0 \tag{21}$$

Utilizing the expression for stress from equation 17 , strain from equation 19 and neutral axis from equation 20, we get the following expression for moment :

$$M = \frac{1}{72} E_1 \kappa t^3 \sqrt{36 - 3t^2\gamma^2\kappa^2} \tag{22}$$

where E_1 is the initial linear stiffness of the composite along the direction of the fibers, which can be approximated by $E_1 = E_0 V_f$ neglecting the contribution of the matrix. The bending stiffness D_{11} is given by :

$$D_{11} = \frac{\partial M}{\partial \kappa} = \frac{E_1 t^3 (6 - t^2\gamma^2\kappa^2)}{12\sqrt{36 - 3t^2\gamma^2\kappa^2}} \tag{23}$$

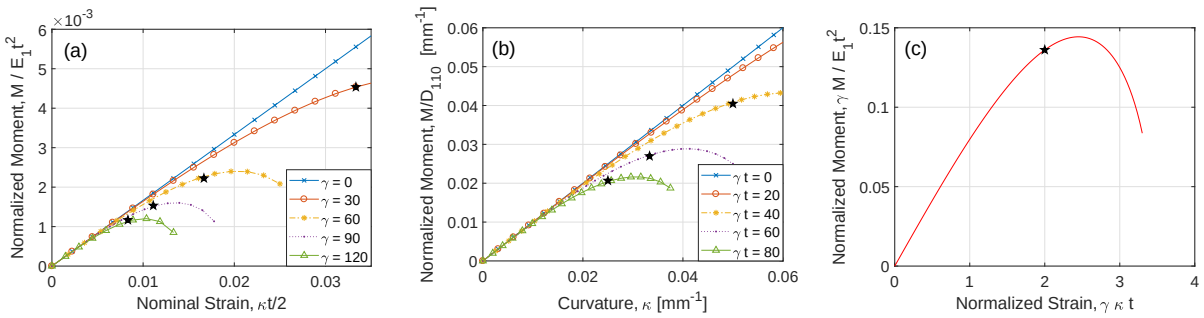

Fig. 5 Plots for normalized moment as a function of a) Nominal strain ($\frac{\kappa t}{2}$), b) Curvature (κ) and c) Nominal strain scaled by 2γ ($\gamma\kappa t$).

Having established the moment vs. curvature relationship in Equation 22 , we observe the trend resulting from three different possible normalizations. Figure 5 plots the expression for normalized moment as a function of nominal strain ($\kappa t/2$), curvature (κ) and nominal strain scaled by 2γ ($\gamma\kappa t$) respectively. Despite the non-standard normalization of the bending moment, this plot is useful because the softening is governed simply by γ, and there is no thickness effect, and so it illustrates the nominal strain at which the behavior deviates from linear for different levels of material softening. We can also see that as γ increases, the critical strain(ε_{cr}) is obtained at a lower nominal strain value. Figure 5b shows the bending moment normalized by the initial bending stiffness, $D_{110} = E_1 t^3/12$, as a function of curvature. In this case the softening is controlled by the parameters γt, and so this can be used as a direct design guideline for picking a given combination of laminate thickness and type of fibers (*i.e.*, a given value of γ). The normalization in Figure 5c incorporates the softening into the normalized strain ($\gamma\kappa t$), allowing for all previous results to collapse into a single master curve.

IV. Analysis using elastica theory

The closed form solution based on the geometric analysis presented in Section II.B assumes a small variation of bending moment across the arclength of the specimen, so that the curvature can be assumed to be constant. If this is not true, the behavior of the coupon needs to be modeled using Euler's theory of elastica, which accounts for large scale deflection of 1D structural elements. We will use the same geometry presented in Figure 3, and for our analysis, Δx is considered to be zero. This not only simplifies the analysis, but leaves only two independent length parameters, the length of the arms, l, and the free length of the sample, l_s.

Assuming that the specimen is inextensible, we utilize the constitutive equation:

$$M(s) = \frac{1}{72} E_1 t^3 \kappa(s) \sqrt{36 - 3t^2\gamma^2\kappa(s)^2} = \frac{1}{72} E_1 t^3 \beta'(s) \sqrt{36 - 3t^2\gamma^2\beta'(s)^2} \tag{24}$$

where $M(s)$ represents the bending moment per unit width at every point along the arclength s, $\kappa(s)$ is the curvature along the arclength, and β represents the angle between the a vector tangent to the coupon and the vertical axis at every point along the curve. In the case of no-softening, $\gamma = 0$, we recover the familiar expression

$$M(s) = D_{110}\kappa(s) = \frac{E_1 t^3}{12}\beta'(s) \tag{25}$$

The differential equations for the position co-ordinates $x(s)$ and $y(s)$ can be given in terms of the angle $\beta(s)$ as:

$$\frac{dx}{ds} = \sin\beta \tag{26}$$

$$\frac{dy}{ds} = \cos\beta \tag{27}$$

For the geometry of the problem, equilibrium of bending moment yields:

$$\frac{1}{72}E_1 t^3 \frac{d\beta}{ds}\sqrt{36 - 3t^2\gamma^2\left(\frac{d\beta}{ds}\right)^2} = M = P\left(x + l\sin\frac{\phi}{2}\right) \tag{28}$$

The above equation can be integrated numerically in Matlab using the 'ode45' command. The boundary conditions are $\theta_{midpoint} = 0$, $x_{midpoint} = x_m$, $x_0 = 0$ and $y_0 = 0$, where x_m represents a vector of specified x-coordinates of the midpoint of the specimen. Since not of all of the conditions can be expressed as initial boundary conditions, a shooting algorithm has been implemented, that calculates the applied loading, as well as the angle rotated by the rigid arms ($\phi/2$) necessary to satisfy the conditions $\theta_{midpoint} = 0$ and $x_{midpoint} = x_m$. The numerical integration provides the shape of the specimen for each applied vertical displacement δ, as well as the distribution of curvature across the arclength, $\kappa(s)$.

V. Comparison of curvature predictions

This section presents a comparison between the curvatures predicted by the closed form equation obtained through the simplified geometric analysis, and the numerical integration of the elastica for four cases involving varying degree of softening of the bent specimen. A preliminary analysis, not using the theory of elastica, was presented previously in [14]. For this study, the thickness is normalized by l_s, and a range of $t/l_s = \{0.005, 0.03\}$ has been used, based on typical values used to test HSC . The values for γ were chosen to vary between 20 and 30, which correspond to the representative values for IM7 and IM10 fibers reported in the literature [21]. Thus, three values for $\frac{\gamma t}{l_s}$ were obtained using the above parameters - 0.1,0.5 and 0.9 and these have been incorporated in the code to obtain the elastica solution for softening. Moreover, for all the cases, it is assumed that $\Delta x = 0$, so the only geometric parameters that appear in the problem are l and l_s. We will define the total arclength of the setup, including the grips, as:

$$L = 2l + l_s \tag{29}$$

Several normalizations have been incorporated here in order to make our results general. First, the curvature has been normalized by l_s. This quantity κl_s represents the approximate angle subtended at the centre of the circle formed by the respective curvature value (in fact, it would be equal to be subtended angle if the curvature was constant). The test displacement has been normalized by L, so that the quantity δ/L represents the relative test displacement with respect to the total arclength L such that the test displacement value does not depend on the coupon freelength or the size of the rigid arms. The theoretical range for δ/L is [0,1], with $\delta/L = 0$ corresponding to the two pins overlapping. The arclength s has been normalized by l_s, so that it varies in the $[0, 1]$ interval.

The geometry of the test can then be defined by a single parameter, the normalized free length ξ, defined as:

$$\xi = \frac{2l}{l_s} \tag{30}$$

which describes the ratio of the size of rigid arms with respect to the specimen freelength. Larger values of ξ correspond to rigid arms that are relatively longer compared to the specimen freelength.

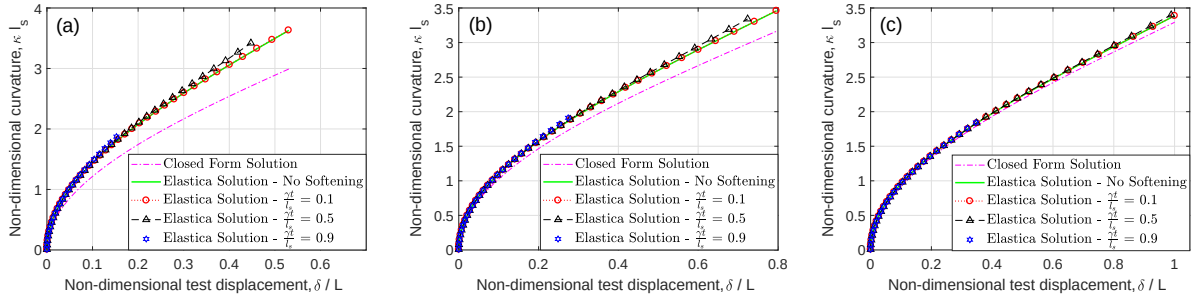

Fig. 6 Curvature as a function of the applied vertical displacement, δ/L, predicted by the geometric solution and the integration of the elastica, for (a) $\xi = 0.5$, (b) $\xi = 2$ and (c) $\xi = 8$.

The maximum curvature predicted by elastica as well as the geometric analysis for different values of ξ is presented in Figure 6, as a function of the normalized vertical displacement during the test, δ/L. The results clearly show that the prediction provided by the closed form solution based on geometric considerations is more accurate for large values of ξ, which corresponds to cases in which the length of the arms is large compared to the coupons. It can also be seen that softening plays a greater role for small values of ξ, where the deviations between the various elastica solutions and the closed form solution is much higher, compared to cases involving larger values of ξ, where the difference between various cases of softening and the non-softening elastica solution, as well as the closed form solution is negligible.

The curvatures presented in Fig. 6 represent the maximum curvature in the sample. Figure 7 presents the nondimensional curvature as a function of the arclength of the sample, for the same three values of ξ and applied vertical displacements of $\delta/L = 0.15$, $\delta/L = 0.25$ and $\delta/L = 0.35$ for $\xi = 0.5$, $\xi = 2$ and $\xi = 8$ respectively. These values for δ/L were chosen based on a test displacement value that was very close to the maximum computationally feasible value that corresponds to a curvature where the fiber modulus becomes zero.

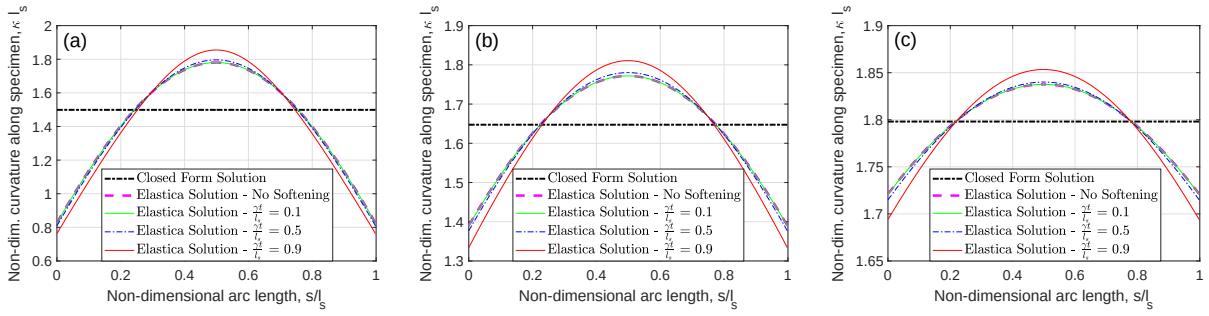

Fig. 7 Variation of the curvature along the arclength, for (a) $\xi = 0.5$; $\delta/L = 0.15$, (b) $\xi = 2$; $\delta/L = 0.25$ and (c) $\xi = 8$; $\delta/L = 0.35$.

Figure 8 shows the error in maximum curvature value, defined as $(\kappa_{max,el} - \kappa_{max,g})/\kappa_{max,el}$, where $\kappa_{max,el}$ and $\kappa_{max,g}$ are the maximum curvature predicted by the elastica and the closed form geometric solution, respectively. For all values of ξ the error slightly increases with the applied displacement, with the effect being more pronounced for smaller values of the ξ. The error is bounded by 5% for $\xi \geq 8$, and by 12% for $\xi \geq 2$, but it can be significant for low values of ξ. All the curvatures have been computed until the curvature value where the fiber modulus becomes zero, and this value is quite low for cases involving higher softening i.e. higher values of γt. This imposes a restriction on the δ/L value upto which the elastica solution for softening can be computed, thereby explaining the lower δ/L value for the same ξ in Figure 8. Another observation that results from the plot is that for smaller values of ξ, softening plays a greater role in the errors involved compared to larger values of ξ. Figure 8 can therefore be used to determine if a given combination of test setup and coupon length can be accurately modeled using the simplified geometric analysis, or if it is necessary to consider curvature variations.

VI. Effect of Softening on the Local Stresses and Strains in the Fibers

In the previous section, the main emphasis was to explore the effect of variation of the ratio of rigid arms to the specimen freelength ξ, and the role it plays in the errors involving computation of curvatures for a thin laminate subjected to flexure. Here, we look at curvature as a way to obtain strain. When there is softening, there is a shift in the neutral axis, such that the maximum strain is no longer $\kappa t/2$. This could have a significant effect even if the change of curvature is not so pronounced. In this section, we will calculate the maximum strains as well as the stresses in the compressive and tensile side, for softening.

Note that all the plots have been plotted against nominal strain ($\kappa t/2$). Doing so eliminates any dependency on thickness, so that all the results hold true regardless of the thickness of the specimen, and the only parameter that varies is γ. Since γ is an empirical parameter whose precise value requires complex testing methodologies, it is essential to investigate its role in the softening of a thin laminate subjected to flexure. In this study, γ is assumed to vary between 20 and 30. This corresponds to the representative values for IM7 and IM10 fibers reported in the literature [21].

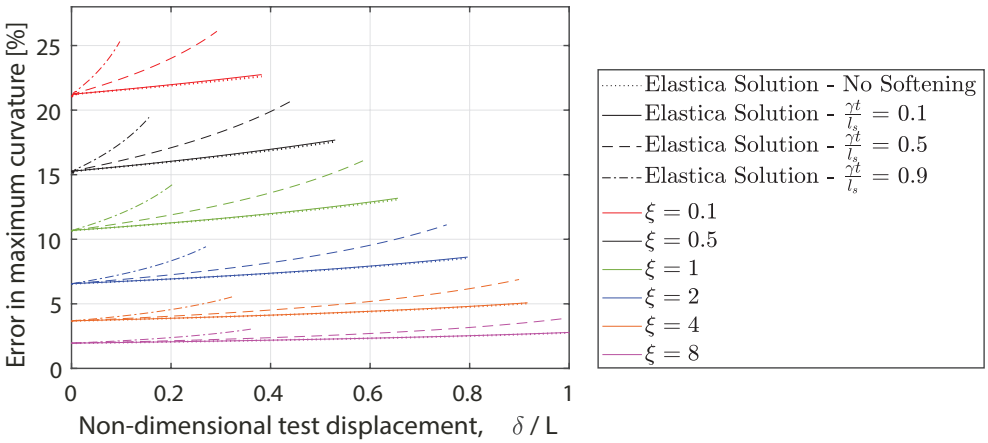

Fig. 8 Error in the prediction of maximum curvature by the closed form geometric solution, as a function of the applied vertical displacement, δ/L, and $\xi = 2l/l_s$.

Figure 9 shows the shift in neutral axis that occurs as a result of varying γ. For a nominal strain of 2%, which is representative of the value at which thin specimens fail, the shift in neutral axis is seen to be 6.7%,8.5% and 10.32%, with respect to half the thickness, for γ values of 20, 25 and 30 respectively. This shift in neutral axis is responsible for the variations in stresses and strains on the tension and compression side.

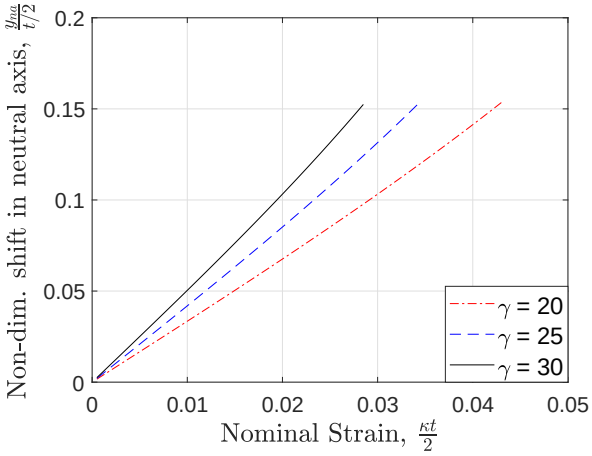

Fig. 9 Comparing the shift in neutral axis as a function of varying γ.

Figure 10 shows the variation in real strain as a function of nominal strain ($\frac{\kappa t}{2}$). The compression side of the specimen experiences larger strains, which occurs as a result of the neutral axis moving towards the tension side, due to tensile stiffening and compression softening. For a nominal strain of 2%, the compression side experiences strains of 2.135%, 2.17% and 2.206% for γ values of 20,25 and 30 respectively, whereas the tension side experiences strains of 1.865%, 1.83% and 1.794% respectively for the same values of γ.

Figure 11 shows the variation of maximum stresses as a function of nominal strain ($\frac{\kappa t}{2}$). Since the contribution of the non-linear term $\frac{\gamma\varepsilon^2}{2}$ to the stress is always positive, the stresses in tension($\varepsilon > 0$) are much higher than stresses in compression($\varepsilon < 0$). For tension, at a nominal strain of 2%, the normalized stress $\frac{\sigma_c}{E_o}$ is 0.02213, 0.02248 and 0.02276 for γ values of 20, 25 and 30 respectively. This corresponds to an error of 2.85% between γ values of 20 and 30, which shows that variation of γ plays a minor role for the evaluation of tensile stresses. Similarly, for compression, at a nominal strain of 2%, the normalized stress $\frac{\sigma_c}{E_o}$ is 0.01679, 0.01582 and 0.01476 for γ values of 20, 25 and 30

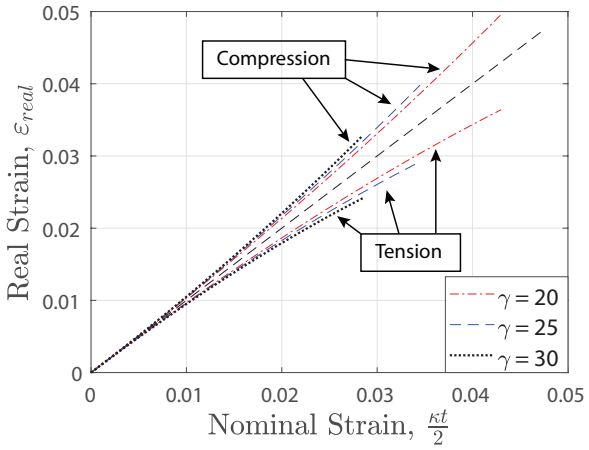

Fig. 10 Comparison of real strains as a function of varying γ.

respectively. This corresponds to an error of 13.75% for γ values of 20 and 30. Hence, variation of γ plays a significant role for the evaluation of compressive stresses, and hence a tighter tolerance for γ needs to be obtained for the desired combination of matrix and fiber.

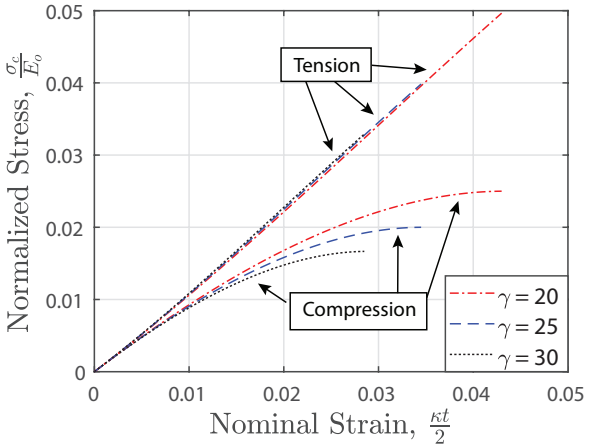

Fig. 11 Comparison of stresses as a function of varying γ.

VII. Experimental validation

In order to validate our analysis, future work will focus on comparison of both the predictions with direct measurements of the curvature obtained by processing images of CBT tests. By taking images of the side of the samples as they are bent, and then processing the images using in-house Matlab codes, it is possible to isolate the pixels corresponding to the sample. These are then used to fit different curves (a circle, and polynomials of order two and three), which are then used to calculate the maximum curvature of the sample. This direct measurement also serves as a validation of the elastica approach, in order to determine discrepancy due to experimental errors.

Preliminary results of the proposed approach are presented in Figure 12(a), corresponding to a sample of unidirectional IM7 fibers, thickness 640μm, and free length l_s = 51.38 mm, corresponding to ξ = 1.2 for the used grips. The figure shows the maximum curvature on the sample, measured at the center of the laminate, as a function of the test displacement. An example of one of the images used to calculate the curvature, as well as the corresponding

fittings, is shown in Figure 12(b). The comparison shows very good agreement between the elastica prediction and the experimental results, with the geometric closed form solution slightly underpredicting the maximum curvature. It should be mentioned that the predictions have not assumed softening, which could explain the small difference between prediction and measurement at high curvatures.

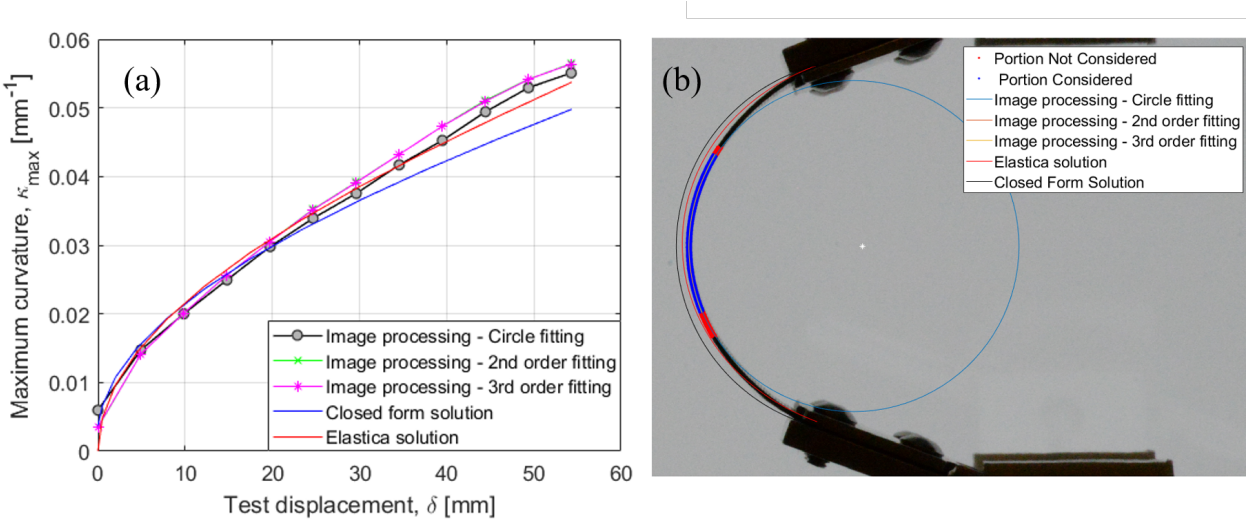

Fig. 12 Experimental results: (a) Comparison of analytical predictions and calculations using test images, and (b) Example of one of the images used to obtain the experimental results, including comparison of different fittings used to estimate the curvature.

VIII. Conclusion

We have analyzed the Column Bending Test, which is used for evaluating the bending behavior of thin flexures under large deformations. Combining the best features of the previously utilized platen test and the large deformation four point bending test, the column bending test loads the coupons with nearly constant bending moment, while avoiding premature failure at the grips. The geometry of the test is such that it allows for simple geometric analysis to approximate the moments and curvatures by assuming that the whole laminate is folded with constant curvature across its arclength. In this paper we have studied the errors associated with this approximation, in particular due to two different effects: changes in the bending moment along the sample, and non-linear material behavior of the fibers, resulting in bending softening at high curvatures.

In order to investigate the effect of the geometry, we first defined a parameter ξ, which measures the ratio between the total size of the rigid arms and the specimen freelength. The bending softening was modeled by accounting for the tension stiffening and compressive softening of the fibers, through a parameter γ whose values are chosen based on experimental observations previously reported in the literature. Our results are produced using Euler's elastica, which accounts for large deflection of 1D structural elements. They show that as ξ increases, the simplified geometric analysis and thus the assumption of the bent coupon as a circle, becomes more and more accurate. This corresponds to the case of a small free-length of the sample, compared to the length of the grips. Also, the softening of the coupon plays a greater role for smaller values of ξ. Differences between the curvature predicted by the elastica and the geometric closed form solution were evaluated for various cases of ξ and γ, providing a design guideline for the geometry of future tests, as a function of the expected failure curvature and material nonlinearity. Overall, the simplified geometric analysis of CBT provides fairly accurate results for larger grip sizes, particularly when the total size of both grips is at least twice the size of coupon freelength, where the error is around 11%.

We also studied the effect of softening of the bent coupon on the local stresses and strains in the fibers due to shift in neutral axis. The shift in neutral axis was found to be between 6.7% and 10.3% for γ values between 20 and 30. This results in a significant variation of the maximum stress in the material, even if the softening does not have a significant effect on the curvature. This indicates that the softening of the fibers need to be taken into account in a predictive model

of the failure of High Strain Composites. More work is required to validate the models for non-linear behavior of fibers, including experiments such as direct testing on single fibers, or measurement of curvature and surface strain in laminates under bending, in order to evaluate the shift in neutral axis.

Currently we are conducting experiments to validate our analysis, using side images of the CBT test and an in-house Matlab image processing code to directly measure the curvature of samples as the test progresses. Preliminary results show good agreement between the observed maximum curvature and that predicted by our elastica analysis, even when material softening is not included, with the geometric closed form solution slightly underpredicting the maximum curvature. Future work will incorporate softening into the analysis, as well as address several experimental difficulties observed in the preliminary test, such as bending of the grips for thick specimens.

Acknowledgments

Funding from Roccor LLC, through the Air Force STTR Program, contract FA9453-17-P-0463, is gratefully acknowledged.

References

[1] McEachen, M., "Validation of SAILMAST Technology and Modeling by Ground Testing of a Full-Scale Flight Article," *48th AIAA Aerospace Sciences Meeting Including the New Horizons Forum and Aerospace Exposition*, 2010, p. 1491.

[2] Mobrem, M., and Adams, D., "Lenticular jointed antenna deployment anomaly and resolution onboard the Mars Express spacecraft," *Journal of Spacecraft and Rockets*, Vol. 46, No. 2, 2009, pp. 403–410.

[3] Baier, H., Datashvili, L., Nathrath, N., and Pellegrino, S., "Technical assessment of high accuracy large space borne reflector antenna," *Final report of ESA contract*, , No. 16757/02, 2004.

[4] Soykasap, O., Pellegrino, S., Howard, P., and Notter, M., "Folding large antenna tape spring," *Journal of Spacecraft and Rockets*, Vol. 45, No. 3, 2008, pp. 560–567.

[5] Pollard, E., and Murphey, T., "Development of deployable elastic composite shape memory alloy reinforced (DECSMAR) structures," *47th AIAA/ASME/ASCE/AHS/ASC Structures, Structural Dynamics, and Materials Conference 14th AIAA/ASME/AHS Adaptive Structures Conference 7th*, 2006, p. 1681.

[6] Spence, B. R., and White, S. F., "Directionally controlled elastically deployable roll-out solar array," , Apr. 1 2014. US Patent 8,683,755.

[7] Murphey, T. W., Francis, W., Davis, B., and Mejia-Ariza, J. M., "High strain composites," *2nd AIAA Spacecraft Structures Conference*, 2015, p. 0942.

[8] Murphey, T. W., Peterson, M. E., and Grigoriev, M. M., "Four point bending of thin unidirectional composite laminas," *54th AIAA/ASME/ASCE/AHS/ASC Structures, Structural Dynamics, and Materials Conference*, 2013, p. 1668.

[9] Yee, J., and Pellegrino, S., "Folding of woven composite structures," *Composites Part A: Applied Science and Manufacturing*, Vol. 36, No. 2, 2005, pp. 273–278.

[10] Sanford, G., Biskner, A., and Murphey, T., "Large strain behavior of thin unidirectional composite flexures," *51st AIAA/ASME/ASCE/AHS/ASC Structures, Structural Dynamics, and Materials Conference 18th AIAA/ASME/AHS Adaptive Structures Conference 12th*, 2010, p. 2698.

[11] Yee, J., and Pellegrino, S., "Biaxial bending failure locus for woven-thin-ply carbon fibre reinforced plastic structures," *46th AIAA/ASME/ASCE/AHS/ASC Structures, Structural Dynamics and Materials Conference*, 2005, p. 1811.

[12] Sanford, G. E., Ardelean, E. V., Murphey, T. W., and Grigoriev, M. M., "High Strain Test Method for Thin Composite Laminates," *16th International Conference on Composite Structures. Porto, Portugal*, 2011.

[13] Jiménez, F. L., and Pellegrino, S., "Folding of fiber composites with a hyperelastic matrix," *International Journal of Solids and Structures*, Vol. 49, No. 3-4, 2012, pp. 395–407.

[14] Rose, T., Sharma, A., Seamone, A., López Jiménez, F., and Murphey, T., "Carbon Unidirectional Composite Flexure Strength Dependence on Laminate Thickness," *Proceedings of the American Society for Composites—Thirty-third Technical Conference*, 2018.

[15] Medina, K., Rose, T., and Murphey, T. W., "Initial Investigation of Time Dependency on Failure Curvatures of FlexLam High Strain Composites," *Proceedings of the American Society for Composites—Thirty-second Technical Conference*, 2017.

[16] Medina, K., Rose, T., and Francis, W., "Long-term Stress Rupture Limitations of Unidirectionasl High Strain Composites in Bending," *Proceedings of the American Society for Composites—Thirty-third Technical Conference*, 2018.

[17] Rose, T., Medina, K., Francis, W., Kawai, K., and Fernandez, J., "Viscoelastic Behaviors of High Strain Composites," *2019 AIAA Spacecraft Structures Conference*, 2019.

[18] Fernandez, J. M., and Murphey, T. W., "A Simple Test Method for Large Deformation Bending of Thin High Strain Composite Flexures," *2018 AIAA Spacecraft Structures Conference*, 2018, p. 0942.

[19] Herrmann, K. M., *An Investigation of a Vertical Test Method for Large Deformation Bending of High Strain Composite Laminates*, 2017.

[20] Murphey, T., Sanford, G., and Grigoriev, M., "Nonlinear elastic constitutive modeling of large strains in carbon fiber composite flexures," *16th International conference on composite structures*, Porto, Portugal: FEUP, 2011.

[21] Murphey, T. W., Peterson, M. E., and Grigoriev, M. M., "Large Strain Four-Point Bending of Thin Unidirectional Composites," *Journal of Spacecraft and Rockets*, Vol. 52, No. 3, 2015, pp. 882–895.

[22] Jones, W., and Johnson, J., "Intrinsic strength and non-Hookean behaviour of carbon fibres," *Carbon*, Vol. 9, No. 5, 1971, pp. 645–655.

[23] Ishikawa, T., Matsushima, M., and Hayashi, Y., "Hardening non-linear behaviour in longitudinal tension of unidirectional carbon composites," *Journal of materials science*, Vol. 20, No. 11, 1985, pp. 4075–4083.

[24] Ueda, M., Saito, W., Imahori, R., Kanazawa, D., and Jeong, T.-K., "Longitudinal direct compression test of a single carbon fiber in a scanning electron microscope," *Composites Part A: Applied Science and Manufacturing*, Vol. 67, 2014, pp. 96–101.